Analytical Expansion of the Dispersion Relation for TLM Condensed Nodes

Vladica Trenkic, *Member, IEEE,* Christos Christopoulos, *Member, IEEE,* and Trevor M. Benson, *Member, IEEE*

***Abstract*— A method for obtaining analytical solutions of the general transmission line modeling (TLM) dispersion relation for condensed node schemes is described. Exact analytical forms of the dispersion relation for currently available nodes are derived, enabling the efficient study of dispersion solutions without resorting to a numerical solver. Using these analytical relations, the range and behavior of propagation errors is fully explored and visualized, not only for propagation along the axes and diagonals or in a coordinate plane, but for arbitrary angles of propagation in three-dimensional space. Comparisons are presented of the numerical performance of different TLM condensed node schemes.**

I. Introduction

MODELING MATERIALS with arbitrary permittivity ε and permeability μ and the use of discretization cells with arbitrary aspect ratio (graded mesh) may be achieved in the transmission line modeling (TLM) method by introducing open- and short-circuit stubs to the conventional symmetrical condensed node (SCN) [1] or by altering the characteristic impedances of the link lines as established in the symmetrical super-condensed node (SSCN) [2]. These two approaches are combined in the hybrid symmetrical condensed nodes (HSCN) [3], [4]. The accuracy of a TLM scheme is dependent on dispersion. The dispersion of the TLM condensed node mesh was originally analyzed in [5] and [6] where a general dispersion relation for the 12-port SCN was derived in the form of an eigenvalue equation. Closed-form solutions to this equation were recently obtained for the SCN without stubs [7], [8] and for the SSCN [9]. Modifications of the general dispersion relation for nodes with stubs can be found in [10]–[16]. The exact analytical formulae for these nodes have so far been obtained only for special cases, namely for propagation in a coordinate plane [9], [12] and along axes and diagonals [16]. A comprehensive numerical study of dispersion was performed in [15], but this was limited to two-dimensional (2-D) propagation only.

In this paper we present a systematic method of deriving dispersion relations algebraically for all condensed nodes in arbitrary propagation directions. We use the method of Faddeev [17] to efficiently compute the required number of leading coefficients of the characteristic polynomial. This analytical expansion of the general TLM dispersion relation facilitates a thorough assessment of the accuracy of available TLM schemes. As a quantitative measure of the deviation from the linear dispersion characteristics of Maxwell's equations, we compute and visualize the propagation error as a function of propagation angles in three-dimensional space. The use of analytical expressions in these computations eliminates potential problems in the separation of two, usually very close, orthogonal solutions, found in the stub-loaded SCN and the HSCN and experienced when using a numerical solver [10]. The results obtained are further checked using simulations of electromagnetic fields in cubic resonators. A detailed comparison of the numerical characteristics of the existing condensed nodes is presented and guidance is offered to users.

Manuscript received December 18, 1995; revised August 26, 1996. This work was supported in part by the Engineering and Physical Sciences Research Council, U.K.

The authors are with the Department of Electrical and Electronic Engineering, University of Nottingham, NG7 2RD Nottingham, U.K.

Publisher Item Identifier S 0018-9480(96)08513-4.

II. Analytical Expansion

The general dispersion relation for the SCN is given as [6]

$$\det(\boldsymbol{PS} - e^{j\theta}\boldsymbol{I}) = 0 \tag{1}$$

where θ is the phase shift along the constituent transmission lines, defined by $\theta = \omega\Delta t$, $\boldsymbol{I}$ is the identity matrix, $\boldsymbol{S}$ is the scattering matrix of the SCN [1], and $\boldsymbol{P}$ is a matrix representing Floquet's theorem [6], which contains the Cartesian components k_x, k_y, k_z of the propagation vector $\vec{k}$. The general dispersion relation (1) can be used for other nodes, provided that the appropriate scattering matrix $\boldsymbol{S}$ is chosen and the matrix $\boldsymbol{P}$ is modified to account for the presence of stubs and mesh grading [10]–[16].

Relation (1) can be solved as an eigenvalue problem, because the left-hand side of (1) represents the characteristic polynomial of the matrix $\boldsymbol{PS}$ in terms of $\psi = \exp(j\theta)$. By obtaining the coefficients $C_i, i = 1 \cdots N$, of this Nth order polynomial, we can write (1) as

$$\mathcal{P}^{(N)}(\psi) = \psi^N + \sum_{i=1}^{N} C_i \psi^{N-i} = 0 \tag{2}$$

where N is equal to the number of node ports. Assuming the presence of $h+l$ nonpropagating solutions of the form $\psi = \pm 1$ and r possible degeneracies of propagating solutions [7], (2) can be written as

$$\mathcal{P}^{(N)}(\psi) = (\psi - 1)^h (\psi + 1)^l (\mathcal{Q}^{(n)}(\psi))^r = 0 \tag{3}$$

where $n = (N - h - l)/r$, which simplifies to

$$\mathcal{Q}^{(n)}(\psi) = \psi^n + \sum_{i=1}^{n} B_i \psi^{n-i} = 0 \tag{4}$$

where $B_{i,i=1\cdots n}$ are coefficients to be determined.

TABLE I
PARAMETERS OF THE CHARACTERISTIC POLYNOMIAL

Node	Case	N	h	l	r	n	m
SCN	—	12	2	2	2	4	2
SSCN	all	12	2	2	2	4	2
HSCN	all	15	2	3	1	10	5
Stub-loaded SCN	1	15	2	3	1	10	5
	2	18	2	0	2	8	4
	3	18	2	0	1	16	8

Case 1: uniform mesh: $\varepsilon_r > 1$, $\mu_r = 1$ or $\mu_r > 1$, $\varepsilon_r = 1$
Case 2: uniform or graded mesh: $\varepsilon_r = \mu_r$
Case 3: uniform or graded mesh: $\varepsilon_r \neq \mu_r$.

Due to symmetry, propagating eigenvalues must appear in reciprocal pairs (ψ, ψ^{-1}), corresponding to propagation in positive and negative directions [8]. Hence it is easily proved that n must be an even number and that the coefficients of $\mathcal{Q}^{(n)}(\psi)$ must be symmetrical, i.e., $B_i = B_{n-i}$ and $B_n = 1$, so that only $m = n/2$ coefficients B_i need to be determined. Dividing (4) by $2\psi^m$ (where $m = n/2$), substituting $B_n = 1$ and $B_{n-i} = B_i$ and making use of $\psi^i + \psi^{-i} = e^{j(i\theta)} + e^{-j(i\theta)} = 2\cos(i\theta)$ for $i = 1 \cdots m$, (4) simplifies to

$$\cos(m\theta) + \sum_{i=1}^{m-1} B_i \cos[(m-i)\theta] + \frac{B_m}{2} = 0. \tag{5}$$

Expression (5) is a general algebraic form of the dispersion relation for propagating solutions. By raising the polynomial $\mathcal{Q}^{(n)}(\psi)$ to the power of r and multiplying by $(\psi-1)^h(\psi+1)^l$, the coefficients B_i can be related to the coefficients C_i of the polynomial $\mathcal{P}^{(N)}(\psi)$. Since only m coefficients B_i are unknown, it is sufficient to obtain the first m coefficients C_i of the characteristic polynomial $\mathcal{P}^{(N)}(\psi)$ to derive the dispersion relation (5). An efficient method for the computation of leading coefficients of the characteristic polynomial is the method of Faddeev [17] described by the following pseudo-code:

Algorithm 1 (Faddeev Method)

$\boldsymbol{A} := \boldsymbol{PS}$;
for $i := 1$ **to** N
begin
$C_i := -\left(\sum_{j=1}^{N} \boldsymbol{A}_{j,j}\right)/i$;
$\boldsymbol{A} := \boldsymbol{PS}, (\boldsymbol{A} + C_i \boldsymbol{I})$
end;

This method has the advantage over conventional diagonalization methods that it can be terminated when a sufficient number of coefficients (m) is computed. Parameters h, l, r, and n appearing in (3) differ for various available nodes. They can be determined by setting fixed, arbitrary numerical values for propagation vector, material properties, and node spacing, so as to obtain numerical roots of $\mathcal{P}^{(N)}(\psi)$ and thus to identify solutions of the form $\psi \pm 1$ and possible degeneracies. These parameters for the presently available nodes are shown in Table I. Note that we separate the analysis of the stubbed SCN into three different cases.

To facilitate a compact formulation of the dispersion relations derived below, we introduce the following substitutions, which will be used throughout the paper:

$$s_1 = c_x + c_y + c_z \qquad s_3 = c_x c_y c_z$$
$$s_2 = c_x c_y + c_y c_z + c_z c_x \qquad s_4 = 2s_1 + s_2$$

with $c_x = \cos(k_x \Delta x) - 1, c_y = \cos(k_y \Delta y) - 1$ and $c_z = \cos(k_z \Delta z) - 1$.

A. Basic 12-Port SCN

To illustrate the proposed methodology, we start by deriving the closed-form dispersion relation of the 12-port SCN. Using data from Table I we write (3) as

$$\mathcal{P}^{(12)}(\psi) = (\psi-1)^2(\psi+1)^2(\mathcal{Q}^{(4)}(\psi))^2 = 0. \tag{6}$$

Since $m = n/2 = 2$, only the first two coefficients of the polynomial $\mathcal{P}^{(12)}(\psi)$ need to be calculated. Using the Faddeev method, coefficients C_1 and C_2 are obtained as $C_1 = 0$ and $C_2 = -2(s_4 + 3)$ where relationships between C_1, C_2 and B_1, B_2 are found by expanding $\mathcal{P}^{(12)}(\psi)$ from (6)

$$C_1 = 2B_1 \qquad C_2 = B_1^2 + 2B_2 - 2 \tag{7}$$

which leads to $B_1 = 0$ and $B_2 = -(s_4 + 2)$. By inserting B_1, B_2 and $m = 2$ into (5) and expanding cosines of multiple angles we obtain the dispersion relation for the SCN as

$$4\cos^2(\theta) = s_4 + 4 \tag{8}$$

which is the relation already derived in [7] and [8].

B. Symmetrical Super-Condensed Node

It can be seen from Table I that the parameters of the characteristic polynomial for the SSCN equal those for the 12-port SCN. Hence, the relationships between B_1, B_2 and C_1, C_2 are given by (7). Using the Faddeev method for the SSCN on uniform mesh we obtain $B_1 = 0$ and $B_2 = -s_4/(\varepsilon_r \mu_r) - 2$ and derive the dispersion relation from (5) as

$$4\varepsilon_r \mu_r \sin^2(\theta) = -s_4. \tag{9}$$

The dispersion relation for the graded SSCN can be obtained in a similar manner and was described in [9].

C. Hybrid Symmetrical Condensed Node

The analytical expansion of the dispersion relation for the hybrid node (HSCN) requires the determination of $m = 5$ coefficients. Due to restricted space, only the algebraic-form dispersion relation for the uniform HSCN mesh is shown here, while expressions for the graded mesh can be found in [18]. The five coefficients B_i required for the dispersion relation (5) can be computed by establishing relationships between coefficients C_i and B_i and applying the Faddeev method to give

$$B_1 = 2(ps_1 + 1)$$
$$B_2 = p^2(s_1^2 + s_2) + 2(p-1)s_4 - 3$$
$$B_3 = p^3(s_1 s_2 - s_3) + 2p(p-1)(s_1^2 + s_1 s_2 + s_2 + 3s_3) - 2p(s_1^2 - s_2) - 4(s_4 + 2)$$

$$
\begin{aligned}
B_4 &= 2p^3(s_1s_2 + s_1s_3 + s_2^2 - s_3) \\
&\quad + p^2(3s_1^2 - 2s_1s_2 - 2s_1s_3 - s_2^2 - s_2 + 6s_3) \\
&\quad - (2p-1)(s_4+1)s_4 + s_4 + 2 \\
B_5 &= 2[p^3(s_1s_2 + 4s_1s_3 + 3s_2s_3 + 3s_3) \\
&\quad + p^2(3s_1^2 - 2s_1s_2 - 2s_1s_3 - s_2^2 - s_2 + 6s_3) \\
&\quad + p(3s_3s_4 - 2s_1s_4 - 2s_1 + 6s_3) \\
&\quad + s_4(s_4+4) + 6] \qquad (10)
\end{aligned}
$$

where $p = 1 - 1/(\varepsilon_r\mu_r)$.

D. Stub-Loaded Symmetrical Condensed Node

In Case 1, when $\mu_r = 1$, the stub-loaded SCN is identical to the HSCN Type I [3], whereas for $\varepsilon_r = 1$ it is identical to the HSCN Type II [4]. Hence, the dispersion relation for the stub-loaded SCN in Case 2 is described by the dispersion relation of the HSCN, derived above.

In Case 2, when $\varepsilon_r = \mu_r$, four coefficients B_i are obtained for the case of uniform mesh as

$$
\begin{aligned}
B_1 &= 2(rs_1 + 2) \\
B_2 &= r^2(3s_2 - 2s_1) + 2r(s_2 + 4s_1) - s_4 + 4 \\
B_3 &= 2r^3(s_3 - 2s_2) + 4r^2(3s_3 + s_2 - 2s_1) \\
&\quad + 2r(-3s_3 + 2s_2 + 7s_1) - 4(s_4+1) \\
B_4 &= 4r^3(-7s_3 - 2s_2) + 2r^2(12s_3 + s_2 - 6s_1) \\
&\quad + 4r(-3s_3 + s_2 + 4s_1) - 2(3s_4 + 5) \qquad (11)
\end{aligned}
$$

where $r = 1 - 1/\sqrt{\varepsilon_r\mu_r}$. The coefficients for a graded mesh can be found in [18].

In Case 3, when $\varepsilon_r \neq \mu_r$, the eight coefficients B_i of the polynomial $\mathcal{Q}^{(16)}(\lambda)$ can be obtained using the Faddeev method. For propagation along a coordinate plane ($k_z = 0$) and using a uniform mesh, this polynomial factorizes as

$$
\mathcal{Q}^{(16)}(\lambda) = (\lambda+1)^2\mathcal{R}_1^{(6)}(\lambda)\mathcal{R}_2^{(6)}(\lambda). \qquad (12)
$$

The coefficients of the polynomial $\mathcal{R}_1^{(6)}(\lambda)$ are

$$
\begin{aligned}
B_1 &= s_1(u+v) + 2 \\
B_2 &= 2s_1(u+v-uv) + s_2(2uv + 2u + v^2) - s_4 - 1 \\
B_3 &= 2[(s_1 + vs_2)(u+v-2uv) - 3s_2uv - s_4 - 2] \qquad (13)
\end{aligned}
$$

where $u = 1 - 1/\varepsilon_r$ and $v = 1 - 1/\mu_r$. The coefficients of the polynomial $\mathcal{R}_2^{(6)}(\lambda)$ are identical to (13) provided that u and v swap places.

For propagation along a diagonal plane ($k_x = k_y$) and using a uniform mesh, the polynomial $\mathcal{Q}^{(16)}(\lambda)$ factorizes as

$$
\mathcal{Q}^{(16)}(\lambda) = \mathcal{R}_1^{(8)}(\lambda)\mathcal{R}_2^{(8)}(\lambda). \qquad (14)
$$

The coefficients of $\mathcal{R}_1^{(8)}(\lambda)$ and $\mathcal{R}_2^{(8)}(\lambda)$ are found in the form

$$
\begin{aligned}
B_1 &= c_x(u+3v) + c_z(u+v) + 4 \\
B_2 &= c_x(c_x + 2c_z)(uv + u + 2v^2 + v - 1) \\
&\quad + c_z(u-v)(2c_xv + 1) \\
&\quad + (2c_x + c_z)(3u + 5v - 2uv - 2) + 4 \\
B_3 &= 2c_x^2c_zv(uv + 3u + 3v - 3) \\
&\quad + 4c_x(c_x + 2c_z)(v^2 - 1)(1-u) + c_x(u-v) \\
&\quad + (2c_x + c_z)(7u + 7v - 8uv - 8) - 4 \\
B_4 &= 2[2c_x^2c_zv(3u + 3v - 7uv - 3) \\
&\quad + c_x(c_x + 2c_z)(-4uv^2 - uv + 3u + 2v^2 - v - 3) \\
&\quad + c_z(2c_xv + 1)(v-u) \\
&\quad + (2c_x + c_z)(5u + 3v - 6uv - 6) - 5]. \qquad (15)
\end{aligned}
$$

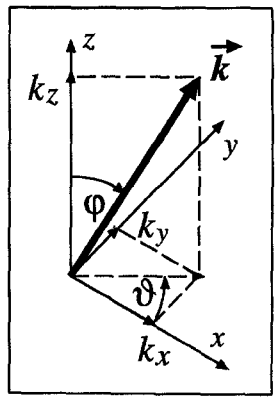

$$\vartheta = \arctan\left(\frac{k_y}{k_x}\right)$$

$$\varphi = \arccos\left(\frac{k_z}{|k|}\right)$$

$$|k| = \sqrt{(k_x^2 + k_y^2 + k_z^2)}$$

Fig. 1. Components of the propagation vector.

III. Quantitative Analysis of Dispersion

The dispersion relations derived here are either linear or quadratic expressions in terms of $\cos(k_x\Delta x), \cos(k_y\Delta y)$ or $\cos(k_z\Delta z)$, thus enabling **exact** analytical computation of the propagation vector $\vec{k}$ for a given ω. We perform our analysis here for the example of uniform mesh with node spacing d and nondissipative isotropic materials with arbitrary ε_r and μ_r. Assuming that the propagation constant in a medium is defined as $k_m = 2\pi/\lambda_0$, where λ_0 is the expected wavelength, we compute θ as $\theta = k_md/(2\sqrt{\varepsilon_r\mu_r})$ [13], choosing a certain discretization level d/λ_0. We then compute, using the dispersion relations, the relative deviation of the propagation vector $\vec{k}$, given by $\delta k' = (|k| - k_m)/k_m$, where $|k| = (k_x^2 + k_y^2 + k_z^2)^{1/2}$.

It has been shown in [19] that all TLM condensed schemes have second-order accuracy, so that when the discretization level (d/λ) is decreased by a factor of two, dispersion error decreases by a factor of four. Therefore, we can normalize the relative deviation $\delta k'$ corresponding to λ_0 to a new value δk, which corresponds to the modeled value of wavelength $\lambda = 2\pi/|k|$, using $\delta k = \delta k'(\lambda/\lambda_0)^2$ [18]. The propagation error δk computed for the benchmark discretization of $d/\lambda = 0.1$ will be denoted by $\overline{\delta k}$ and it is investigated for different angles of propagation φ, ϑ defined as $\vartheta = \arctan(k_y/k_x)$ and $\varphi = \arccos(k_z/|k|)$, as depicted in Fig. 1.

For validation purposes, the propagation error δk can also be calculated from the numerical simulation of resonators and waveguides by $\delta k = (f_0 - f)/f$, where f_0, f are the physical and modeled frequencies, respectively [18].

The propagation error $\overline{\delta k}$ for the 12-port SCN, calculated from the dispersion relation (8) is illustrated in Fig. 2 using contour and surface plots. The contour plot shows this error for angles $0 \leq \varphi, \vartheta \leq 90°$. It can be seen that maximum error occurs for propagation along the main space diagonal [**111**].

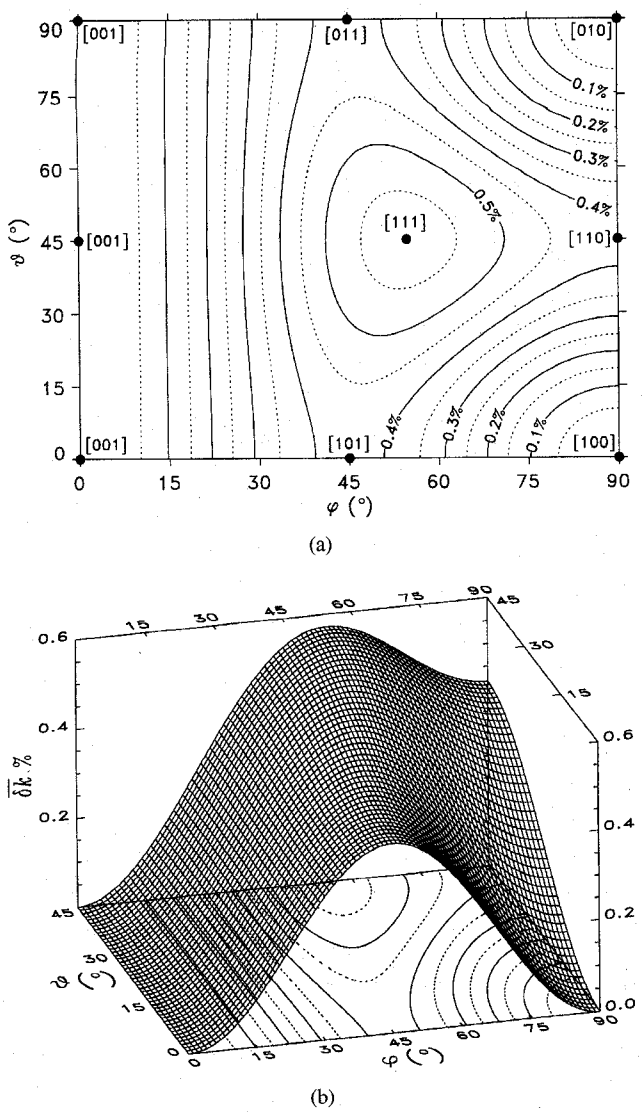

Fig. 2. Propagation error in SCN ($\varepsilon_r \mu_r = 1$).

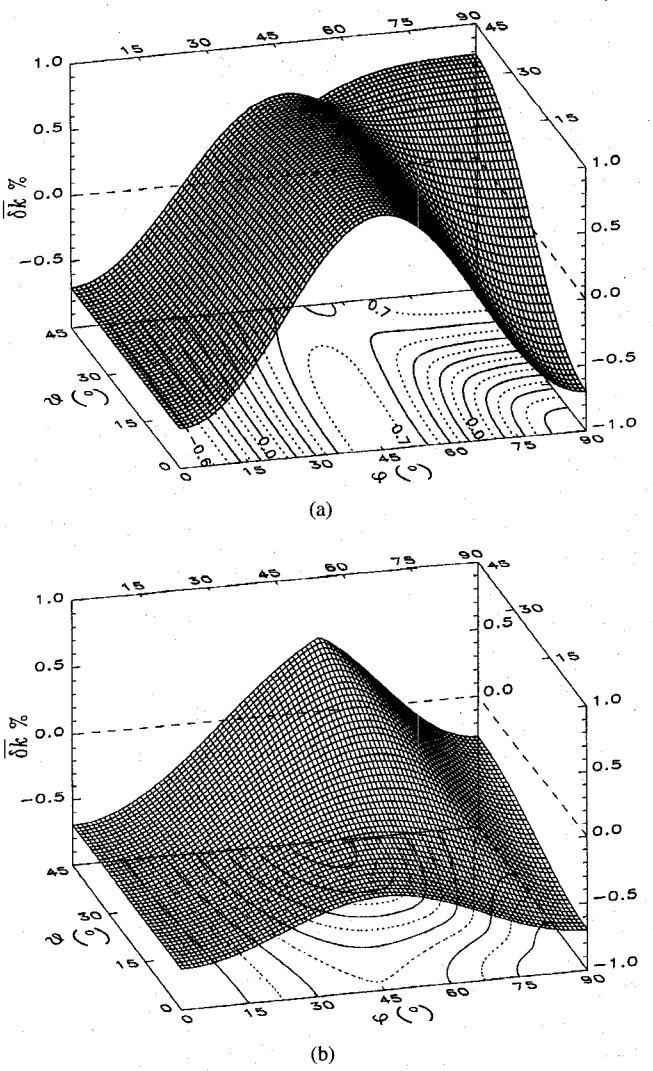

Fig. 3. Propagation error in stub-loaded SCN Case 1 and HSCN for $\varepsilon_r \mu_r = 8$. (a) TM and (b) TE modes for the stub-loaded node modeling a dielectric ($\varepsilon_r = 8$) and for the Type I HSCN. (a) TE and (b) TM modes for the stub-loaded node modeling a magnetic medium ($\mu_r = 8$) and for the Type II HSCN.

Because of the symmetry, $\overline{\delta k}$ is shown in the surface plot of Fig. 2 only for angles $0 \leq \vartheta \leq 45°$. A cross section of the surface plot for $\vartheta = 0$ gives information on the propagation errors along a coordinate plane, in this case $y = 0$, and contains directions [**u0v**]. A cross section for $\vartheta = 45°$ gives these errors for propagation along a diagonal plane, in this case $x = y$, and contains directions [**uuv**].

A. *Stub-Loaded SCN in Case 1 and HSCN*

With coefficients obtained from (10), the dispersion relation (5) is a quadratic equation in $\cos(k_x d), \cos(k_y d)$ or $\cos(k_z d)$, which yields two solutions, corresponding to two orthogonal wave polarizations. For the case of propagation in the xy-plane these solutions contain components E_z, H_x, H_y or H_z, E_x, E_y [12], which subsequently are referred to as TE and TM modes, respectively. These two orthogonal solutions are plotted in terms of the propagation error $\overline{\delta k}$ for $\varepsilon_r \mu_r = 8$ in Fig. 3(a) and (b).

We now analyze the dispersion for propagation in coordinate ($k_y = 0$) and diagonal ($k_x = k_y$) planes, defined as subcases (a) and (b), respectively. Note that for subcase (a), (5) with coefficients (10) simplifies into two separate dispersion relations for TE and TM modes, presented in [9]. Fig. 4(a) and (b) shows the propagation error $\overline{\delta k}$ in the stub-loaded SCN in Case 1 and the HSCN for subcases (a) and (b). The upper and lower sets of curves in Fig. 4(a) and (b) correspond to TM and TE solutions of (5) for the stub-loaded SCN modeling a dielectric ($\mu_r = 1$) and for the Type I HSCN. The opposite interpretation of the solutions is valid for the stub-loaded SCN modeling magnetic media ($\varepsilon_r = 1$) and for the Type II HSCN.

Different directions of propagation can be studied in Fig. 4(a) and (b), some of which are marked on the x-axis. Both parts of Fig. 4 show the coexistence of positive and negative propagation errors, described in [12] as "bilateral dispersion." The two sets of curves representing orthogonal solutions of (5) converge for axial propagation [Fig. 4(a)] and propagation along the main space diagonal [Fig. 4(b)].

B. *Stub-Loaded SCN in Case 2*

With coefficients obtained from (11), dispersion relation (5) is a linear equation in $\cos(k_x d), \cos(k_y d)$ or $\cos(k_z d)$, yielding

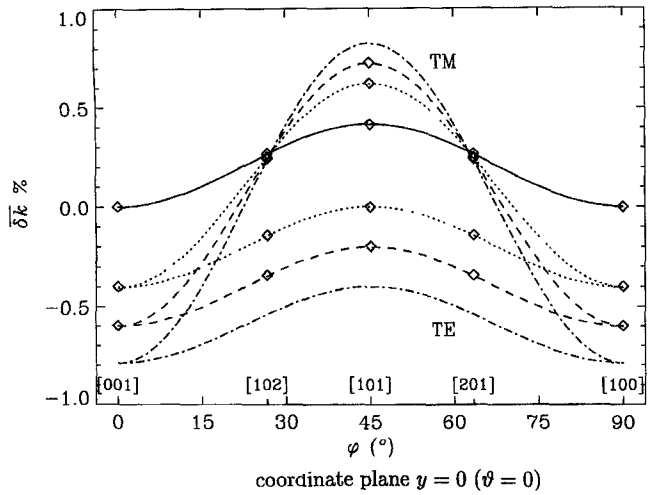

(a)

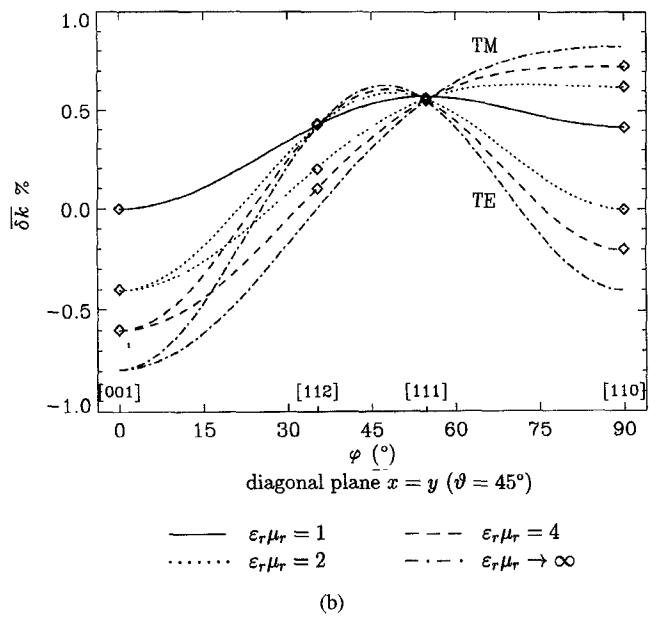

(b)

Fig. 4. Propagation error in stub-loaded SCN Case 1 and the HSCN for subcases (a) and (b).

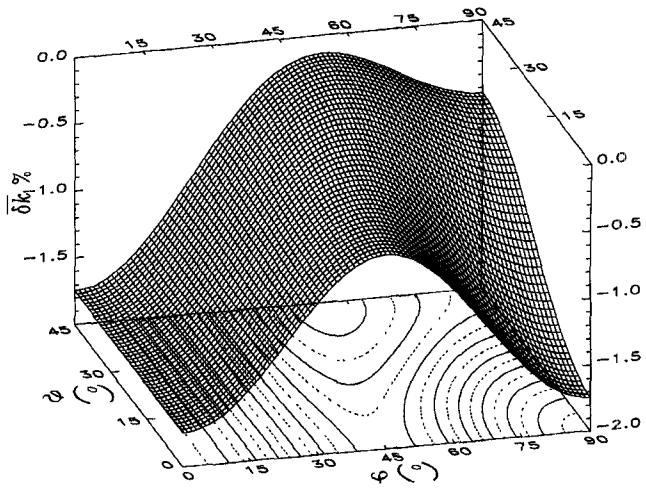

Fig. 5. Propagation error in stub-loaded SCN Case 2 for $\varepsilon_r\mu_r = 8$.

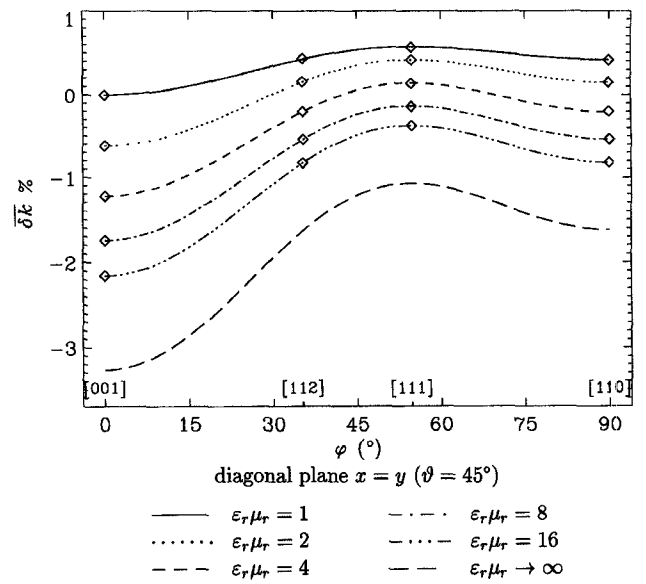

Fig. 6. Propagation error in stub-loaded SCN Case 2(b).

a single dispersion solution, which confirms numerical results in [12]. A solution of (5) in terms of the propagation error $\overline{\delta k}$ for $\varepsilon_r\mu_r = 8$ is shown in Fig. 5.

Fig. 6 shows the propagation error in the stubbed SCN for Case 2(b). It shows that $\overline{\delta k}$ is significantly higher than in Case 1, and that the highest error occurs for axial propagation (e.g., [001]). The solutions at a given frequency converge when $\varepsilon_r\mu_r \to \infty$ but at a slower rate than in Case 1. The propagation error is bilateral for smaller $\varepsilon_r\mu_r$ and negative for higher $\varepsilon_r\mu_r$.

C. Stub-Loaded SCN in Case 3

Fig. 7(a) and (b) shows the propagation error in the stub-loaded SCN for Cases 3(a) and (b), respectively, for $\varepsilon_r\mu_r = \text{const} = 8$, computed by using (13) and (15). Note that the three curves corresponding to values $\varepsilon_r, \mu_r \geq 2$ are very close, indicating that the propagation error for Case 3 for higher values of ε_r, μ_r is similar to that in Case 2, unless $\varepsilon_r \to 1$ or $\mu_r \to 1$ when Case 3 converges to Case 1. As in Case 1, swapping values of ε_r and μ_r swaps orthogonal solutions for TE and TM modes.

D. Symmetrical Super-Condensed Node

The propagation error $\overline{\delta k}$ in the SSCN for $\varepsilon_r\mu_r = 8$ is computed from (9) and is shown in Fig. 8. The surface $\overline{\delta k}(\varphi, \vartheta)$ in Fig. 8 has the same shape as the related surface for the 12-port SCN shown in Fig. 2 with $\overline{\delta k}$ shifted by around 1.45%. Fig. 9 shows that the propagation error for the SSCN is always positive (i.e., unilateral) and is largest for propagation along the main space diagonal. The curves for different $\varepsilon_r\mu_r$ are uniformly shifted, which means that the range of propagation error within an individual medium is constant.

IV. Validation

The analytical expressions presented here have been checked against results from the eigenvalue analysis of cubic resonators, using a simulation procedure similar to that of [12]. Assuming that the wavelength λ is imposed by the boundary

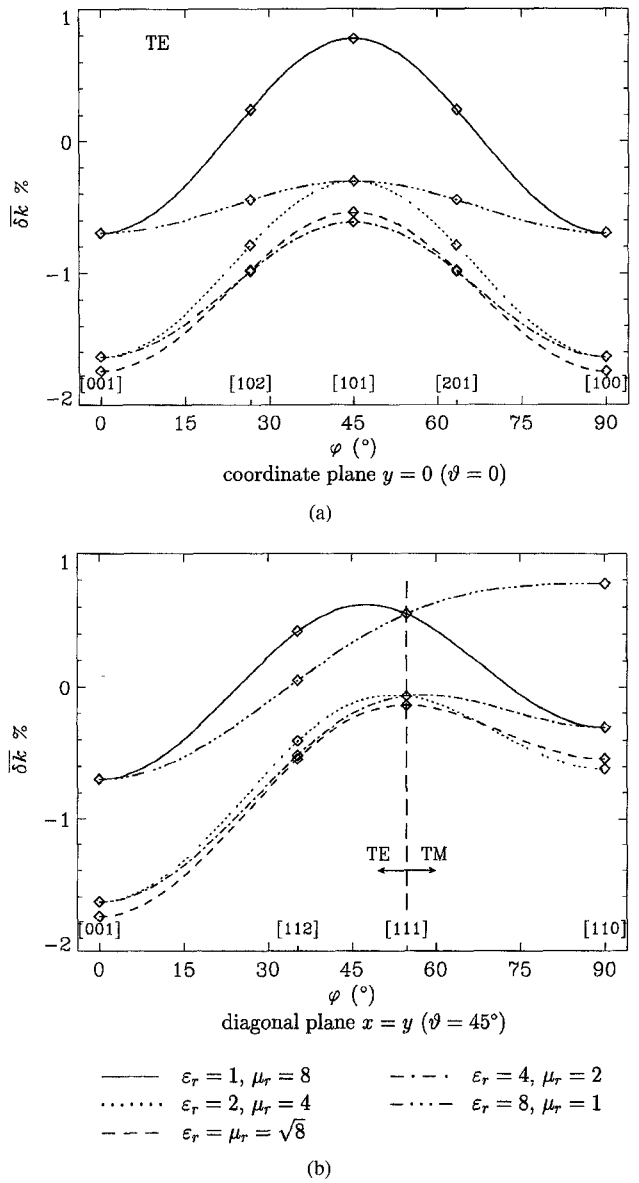

Fig. 7. Propagation error in stub-loaded SCN for Cases 3(a),(b).

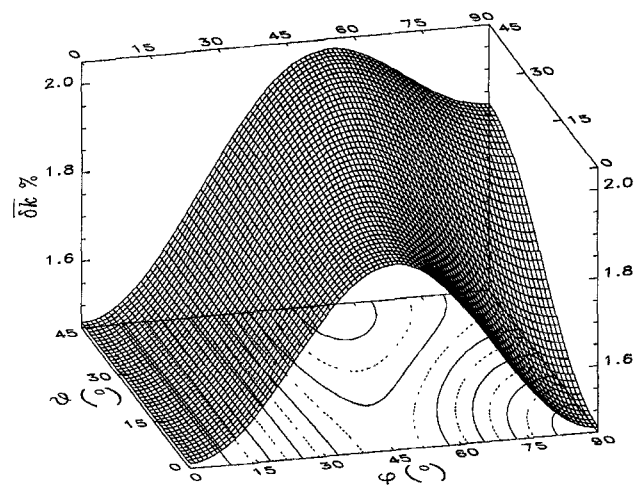

Fig. 8. Propagation error in SSCN for $\varepsilon_r \mu_r = 8$.

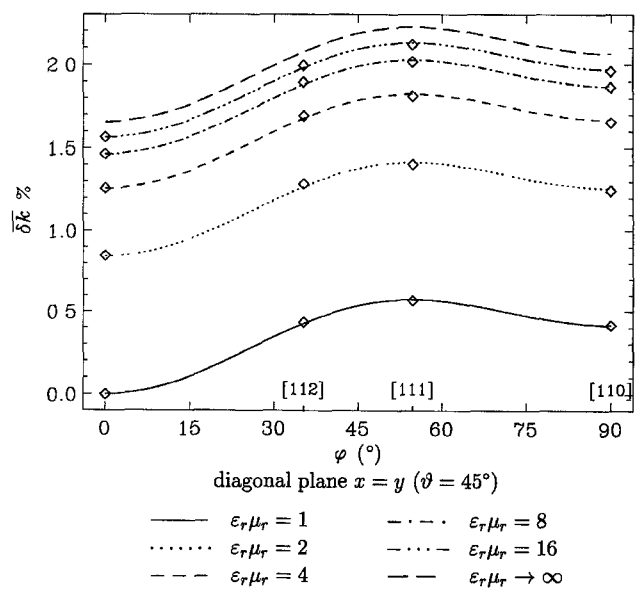

Fig. 9. Propagation error in SSCN for subcase (b).

conditions of a resonator and following the definitions and discussion in Section II, the propagation error $\overline{\delta k}$, normalized further to account for the fact that $d/\lambda \neq 0.1$, is computed by

$$\overline{\delta k} = \left(\frac{f_0}{f} - 1\right)\left(\frac{0.1}{d/\lambda}\right)^2. \tag{16}$$

Note that a positive $\overline{\delta k}$ means that f underestimates f_0. Numerical results are marked with diamond symbols and plotted in Figs. 4, 6, 7, and 9 for different propagation directions. They are found to be in excellent agreement with the analytical plots. Spurious propagating solutions described in [6] and [7] do not show significant impact on the results obtained from these simulations.

V. Comparisons

A summary of the numerical characteristics of the existing condensed nodes is shown in Table II. The properties of the 12-port SCN are also shown as reference, although this node cannot model inhomogeneous media.

The first set of rows of Table II concerns the nature of the dispersion. In TLM, errors due to dispersion depend normally on the discretization (d/λ), wave velocity $(1/\sqrt{\varepsilon\mu})$ and direction of propagation (ϑ, φ). The two orthogonal solutions of (5) for the stub-loaded SCN and the HSCN reveal that dispersion for these nodes is further dependent on the wave polarization. This can have the effects of splitting degenerate modes, which would otherwise have the same resonant frequencies, and changing the polarization of propagating waves [11]. The dispersion in the stub-loaded SCN is also function of the medium impedance, i.e., it depends on μ_r/ε_r for $\mu_r\varepsilon_r = \text{const}$ and both the stub-loaded SCN and the HSCN experience bilateral dispersion [12]. In contrast, the nature of the dispersion errors in the SSCN is identical to that of the basic SCN, i.e., dispersion is independent of the wave polarization and of the medium impedance and the error is unilateral. These are regarded as advantageous features of the SSCN.

The second set of rows of Table II shows maximum propagation errors calculated for a discretization of $d/\lambda =$

TABLE II
NUMERICAL CHARACTERISTICS OF VARIOUS TLM CONDENSED NODE SCHEME

Node	SCN	Stub-loaded SCN			HSCN	SSCN
		Case 1	Case 2	Case 3		
Dispersion independent of the wave polarization	Yes	No	Yes	No	No	Yes
Dispersion independent of the medium impedance	Yes	No	Yes	No	Yes	Yes
Unilateral propagation error	Yes	No	No	No	No	Yes
Max. positive propagation error $\overline{\delta k}_{\max+}$ (%)	0.57	0.83	0.57	0.83	0.83	2.22
Max. negative propagation error $\overline{\delta k}_{\max-}$ (%)	0.00	0.79	3.26	3.26	0.79	0.00
Total error range, $\overline{\delta k}_t = \overline{\delta k}_{\max+} + \overline{\delta k}_{\max-}$ (%)	0.57	1.62	3.83	4.09	1.62	2.22
Storage N (locations per node)	12	15	18	18	15	12
Total error range $\overline{\delta k}_{t,18}$ normalized to $N = 18$ (%)	0.44	1.43	3.83	4.09	1.43	1.69
MUL operations per node per iteration	6	9	12	12	12	6
ADD/SUB operations per node per iteration	24	48	54	54	48	48

0.1, for all propagation angles and all media with properties $1 \leq \varepsilon_r \mu_r < \infty$. Table II shows that the total error range $\overline{\delta k}_t$, defined as in [12], is the highest in the stub-loaded SCN in Cases 2 and 3. In order to compare further the performance of various nodes, the error range $\overline{\delta k}_t$ is normalized to $N = 18$ storage locations per node by multiplying it with (N/18) raised to the power of two (second-order accuracy) and 1/3 (three-dimensional mesh) to produce $\overline{\delta k}_{t,18} = \overline{\delta k}_t (N/18)^{2/3}$. Effectively, $\overline{\delta k}_{t,18}$ represents the error range for each node assuming the same total storage and it is smallest for the HSCN. However, the SSCN is more computationally efficient as it uses only six multiplicative (MUL) operations per node per time step for the scattering procedure [20].

Further consideration should be given to dispersive effects at interfaces between nodes modeling different materials. The impact of mesh grading may be studied using the same approach as described in Section II. The effect of mesh grading is to introduce different behavior in different directions, however, the error range is similar to that for uniform mesh [18], [21]. In general, the optimum TLM condensed node scheme is problem dependent and data in Table II offer a general guidance as to what may be achievable in each case. It appears that when modeling dielectric materials, the stub-loaded SCN and the HSCN are the most accurate and reasonably efficient, but degenerate modes are likely to be split. For the general case $(\varepsilon_r, \mu_r > 1)$, the HSCN offers the best accuracy, whereas the SSCN offers a higher efficiency and identical dispersion for TE and TM modes.

VI. CONCLUSION

Using a systematic algebraic procedure, analytical expansion of the general TLM dispersion relation was made possible for different symmetrical condensed nodes capable of modeling media with arbitrary electromagnetic parameters. Efficient ways of studying and visualizing dispersion errors were presented and a detailed quantitative analysis and comparison of the results were performed. The analytical results obtained by solving dispersion relations were validated against modeled results.

The dispersion analysis presented here can be combined with the theoretical foundation of the general symmetrical condensed node [19] in order to explore possibilities of deriving new TLM schemes with better propagation characteristics. Given the theoretical instrument to describe new nodes and a systematic analytical procedure to study their accuracy, further work will be directed toward the development of such more advanced TLM formulations. A comprehensive comparison between the available TLM and finite-difference schemes will also be subject of the future work.

REFERENCES

[1] P. B. Johns, "A symmetrical condensed node for the TLM method," *IEEE Trans. Microwave Theory Tech.*, vol. MTT-35, no. 4, pp. 370–377, Apr. 1987.

[2] V. Trenkic, C. Christopoulos, and T. M. Benson, "Theory of the symmetrical super-condensed node for the TLM method," *IEEE Trans. Microwave Theory Tech.*, vol. 43, no. 6, pp. 1342–1348, June 1995.

[3] R. A. Scaramuzza and A. J. Lowery, "Hybrid symmetrical condensed node for TLM method," *Electron. Lett.*, vol. 26, no. 23, pp. 1947–1949, Nov. 1990.

[4] P. Berrini and K. Wu, "A pair of hybrid symmetrical condensed TLM nodes," *IEEE Microwave Guided Wave Lett.*, vol. 4, no. 7, pp. 244–246, July 1994.

[5] J. S. Nielsen and W. J. R. Hoefer, "A complete dispersion analysis of the condensed node TLM mesh," *IEEE Trans. Magn.*, vol. 27, no. 5, pp. 3982–3985, Sept. 1991.

[6] ——, "Generalized dispersion analysis and spurious modes of 2-D and 3-D TLM formulations," *IEEE Trans. Microwave Theory Tech.*, vol. 41, no. 8, pp. 1375–1384, Aug. 1993.

[7] M. Krumpholz and P. Russer, "On the dispersion in TLM and FDTD," *IEEE Trans. Microwave Theory Tech.*, vol. 42, no. 7, pp. 1275–1279, July 1994.

[8] V. Trenkic, T. M. Benson, and C. Christopoulos, "Dispersion analysis of a TLM mesh using a new scattering matrix formulation," *IEEE Microwave Guided Wave Lett.*, vol. 5, no. 3, pp. 79–80, Mar. 1995.

[9] V. Trenkic, C. Christopoulos, and T. M. Benson, "Dispersion analysis of TLM symmetrical super-condensed node," *Electron. Lett.*, vol. 30, no. 25, pp. 2151–2153, Dec. 1994.

[10] D. P. Johns and C. Christopoulos, "Dispersion of time-domain and frequency domain formulations of the symmetrical condensed TLM node," in *2nd Int. Conf. Computation in Electromagnetics*, Nottingham, U.K., Apr. 1994, pp. 295–298, IEE Conf. publ. 384.

[11] M. Celuch-Marcysiak, "Toward better understanding of the SCN TLM method for inhomogeneous problems," in *2nd Int. Workshop on Discrete Time Domain Modeling of Electromagnetic Fields and Networks*, Berlin, Germany, Oct. 1993.

[12] M. Celuch-Marcysiak and W. K. Gwarek, "On the effect of bilateral dispersion in inhomogeneous symmetrical condensed node modeling," *IEEE Trans. Microwave Theory Tech.*, vol. 42, no. 6, pp. 1069–1073, June 1994.

[13] V. Trenkic, C. Christopoulos, and T. M. Benson, "Dispersion of TLM condensed nodes in media with arbitrary electromagnetic properties," in *IEEE Int. Microwave Symp. Dig.*, Orlando, Florida, May 1995, vol. 2, pp. 373–376.

[14] J. A. Morente, G. Gimenez, A. Porti, and M. Khalladi, "Dispersion analysis for a TLM mesh of symmetrical condensed nodes with stubs," *IEEE Trans. Microwave Theory Tech.*, vol. 43, no. 2, pp. 452–456, Feb. 1995.

[15] P. Berini and K. Wu, "A comprehensive study of numerical anisotropy and dispersion in 3-D TLM meshes," *IEEE Trans. Microwave Theory Tech.*, vol. 43, no. 5, pp. 1173–1181, May 1995.

[16] C. Huber, M. Krumpholz, and P. Russer, "Dispersion in anisotropic media modeled by three-dimensional TLM," *IEEE Trans. Microwave Theory Tech.*, vol. 43, no. 8, pp. 1923–1934, Aug. 1995.

[17] F. R. Gantmacher, *The Theory of Matrices*. New York: Chelsea, 1959, ch. 4, pp. 87–89.

[18] V. Trenkic, "Development and characterization of advanced nodes for the TLM method," Ph.D. thesis, Univ. of Nottingham, U.K., 1995.

[19] V. Trenkic, C. Christopoulos, and T. M. Benson, "Development of a general symmetrical condensed node for the TLM method," *IEEE Trans. Microwave Theory Tech.*, vol. 44, no. 12, pp. 2129-2135, Dec. 1996.

[20] ——, "Efficient computational algorithms for TLM," in *First Int. Workshop on Transmission Line Matrix (TLM) Modeling Dig.*, Victoria, Canada, Aug. 1995, pp. 77–80.

[21] ——, "On the time step in hybrid symmetrical condensed TLM nodes," *IEEE Trans. Microwave Theory Tech.*, vol. 43, no. 9, pp. 2172–2174, Sept. 1995.

Vladica Trenkic (M'96), for a photograph and biography, see this issue p. 2135.

Christos Christopoulos (M'92), for a photograph and biography, see this issue p. 2135.

Trevor M. Benson (M'96), for a photograph and biography, see this issue p. 2135.